Model-driven segmentation of X-ray left ventricular angiograms

Oost, C.R.

改心
'improvement'

Chapter 3

Multi-View Active Appearance Models: Application to X-Ray LV Angiography and Cardiac MRI

This chapter was adapted from:
Multi-View Active Appearance Models: Application to X-Ray LV Angiography and Cardiac MRI
C.R. Oost, B.P.F. Lelieveldt, M. Üzümcü, H. Lamb, J.H.C. Reiber, and M. Sonka
In: Proceedings of IPMI 2003, C.J. Taylor and J.A. Noble Eds., vol. 2732, pp. 234-245, 2003.

Abstract

This chapter describes a Multi-View Active Appearance Model (AAM) for coherent segmentation of multiple cardiac views. Cootes' AAM framework was adapted by considering shapes and intensities from multiple views as single shape and intensity samples, while eliminating trivial difference in object pose in different views. This way, the coherence in organ shape and intensities between different views is modeled, and utilized during image search. The method is validated in two substantially different and novel applications: segmentation of combined end-diastolic and end-systolic X-ray left ventricular angiograms, and simultaneous segmentation of a combination of four chamber, two chamber and short-axis cardiac MR views.

3.1 Introduction

In cardiac imaging, typically multiple acquisitions are acquired within one patient examination following fixed imaging protocols, where images may depict different geometrical or functional features of the heart. For instance, in cardiac MR imaging, the short-axis, long-axis, perfusion, rest-stress and delayed enhancement images provide complementary information about different aspects of geometry and function of the same heart. Also, in bi-plane X-ray left ventricular (LV) angiography, different views are acquired of the LV, which are the left anterior oblique 60° and right anterior oblique 30°, showing the left ventricle from different projection angles. Different time frames from an angiographic or echographic image sequence are other examples of such interrelated views.

To quantify cardiac function and morphology from such image sets, a (preferably automatic) segmentation of the heart is required. However, typically, automatic segmentation methods focus on one subpart of a patient examination. Segmentation is achieved for one view at a time, and the different parts of a patient examination are treated separately. As a result, not all available information is used to achieve a segmentation result, since additional shape information of the same organ may be available from a different view. The goal of this work was to develop a segmentation method that exploits existing shape and intensity redundancies and correlations between different parts of a patient examination. Potentially, this increases robustness, and enforces segmentation consistency between views, therefore yielding a better segmentation.

To realize this, we have developed the Multi-View Active Appearance Model (AAM): an extension of Cootes' AAM framework [1-5] that captures the coherence and correlation between multiple parts of a patient examination. Model training and matching are performed on multiple 2D views simultaneously, combining information from all views to yield a segmentation result. To investigate the clinical potential, we validate the Multi-View AAM in two substantially different, largely unsolved segmentation problems: automatic definition of the LV contours in pairs

of X-ray LV angiograms in ED and ES phase, and second, simultaneous LV contour detection in a combination of short-axis, four and two chamber cardiac MR views.

3.2 Background

An Active Appearance Model is a statistical model of object shape and texture. The construction of the AAM and the matching procedure are briefly introduced in this section. A detailed description can be found in [3].

3.2.1 AAM Training

An AAM is trained on a series of representative images, in which an expert manually segmented the object of interest. Contours are resampled in n corresponding points, and, for the 2D case, expressed as a vector of $2n$ elements:

$$\mathrm{x} = \left(x_1, y_1, x_2, y_2, x_3, y_3, \ldots, x_n, y_n\right)^T \tag{3.1}$$

After Procrustes alignment of the shape vectors to eliminate trivial pose differences, a shape model is built by applying Principal Component Analysis (PCA) on the sample covariance matrix. Arranging the eigenvectors according to descending eigenvalues enables elimination of less significant eigenvectors.

Similarly, a texture model is created by warping the training images onto the mean shape and creating a shape free patch, from which pixel intensity vectors g are extracted. Texture vectors are normalized to zero average and unit variance and PCA is performed on the sample covariance matrix, resulting in the statistical texture model. Using the shape and texture models, the sample shapes x and textures g can be approximated from the respective models:

$$\mathrm{x} \approx \bar{\mathrm{x}} + P_s b_s \quad \text{and} \quad \mathrm{g} \approx \bar{\mathrm{g}} + P_g b_g \tag{3.2}$$

where $\bar{\mathrm{g}}$ and $\bar{\mathrm{x}}$ represent the average texture and shape vectors, P_g and P_s the texture and shape eigenvector matrices, and b_g and b_s the texture and shape parameters characterizing each training sample.

From the shape and texture models, an AAM is created by concatenating the shape and texture parameter vectors:

$$b = \begin{pmatrix} W b_s \\ b_g \end{pmatrix} = \begin{pmatrix} W P_s^T \left(\mathrm{x} - \bar{\mathrm{x}}\right) \\ P_g^T \left(\mathrm{g} - \bar{\mathrm{g}}\right) \end{pmatrix} \tag{3.3}$$

W denotes a weight factor coupling the shape and texture coefficients.

After a final PCA over the set of appearance vectors b the resulting AAM can be written as:

$$b = Qc \tag{3.4}$$

in which Q is the matrix containing the eigenvectors and c denotes the appearance parameters for the combined model.

Matching the model to an unseen image involves minimizing the root mean square error between the model generated image and the target image, within the boundaries of statistically plausible model limits. To drive the model matching iterations the parameter update steps are computed from the residual images $\delta g_0 = g_s - g_m$, where g_s denotes the target image, and g_m the model synthesized image. By applying known parameter perturbations on model, pose and texture, gradient matrices R_c, R_p and R_t can be estimated for model, pose and texture respectively. In our approach, we adopted the direct gradient method by Cootes *et al.* [5].

3.2.2 AAM Matching

From the current estimate of the model parameters c_o and the parameter derivatives for the model, texture and pose parameters (matrices R_c, R_t & R_p respectively), Cootes describes an iterative matching algorithm, consisting of the following steps [2]:

1) Calculate the residual between target image and model patch $\delta g_0 = g_s - g_m$

2) Calculate the RMS error from the difference-vector $E_0 = |\delta g_0|^2$

3) Using the pre-computed gradient matrices, determine the model parameter update $\delta c = R_c \delta g_0$, pose update $\delta p = R_p \delta g_0$ and texture update $\delta t = R_t \delta g_0$

4) Set k = 1 and determine a new estimate for the model parameters $c_1 = c_0 - k\delta c$, pose parameters $p_1 = p_0 - k\delta p$ and texture parameters $t_1 = t_0 - k\delta t$

5) Calculate a new model based on c_1, p_1 & t_1

6) Determine a new difference-vector and calculate its RMS error E_1,

7) If $E_1 < E_o$, select c_1, p_1 & t_1 as the new parameter vectors, else try k = 1.5, k = 0.5, k = 0.25 etc. and go to step 4

Repeat until convergence (either using a fixed number of iterations, or until no improvement is achieved).

3.2.3 Medical Applications of AAMs

Since introduction, several successful medical applications of AAMs in medical image segmentation have been presented. Initially, Cootes has demonstrated the application of 2D AAMs on finding structures in brain MR images [2], and knee cartilage in MR images [3]. In 2D cardiac MR images, Mitchell *et al.* successfully applied AAMs to segment the left and right ventricle [6]. Thodberg [7] applied a 2D AAM to reconstruct bones in hand radiographs. Bosch *et al.* applied a 2D + time AAM to segment endocardial borders in echocardiography [8], introducing a correction method to compensate for non-Gaussian intensity distributions in echocardiographic images. Beichel *et al.* described a semi-3D AAM extension applied to the segmentation of the diaphragm dome in 3D CT data [9]. Mitchell *et al.* described a full 3D AAM extension, and applied it to 3D cardiac MR data and 2D + time echocardiograms [10].
In many of the applications mentioned here, Active Appearance Models have been shown to outperform other segmentation approaches for two reasons:

- They combine correlated intensity and shape knowledge, thus maximally integrating a priori knowledge, resulting in highly robust performance.

- They model the relationship between expert contours and underlying image data, and are therefore capable of reproducing expert contour drawing behavior.

3.3 Multi-View Active Appearance Models

The Multi-View AAM presented here is designed to exploit the existing correlation between different views of the same object. It is derived from Cootes' work on coupled view AAMs [4], where a frontal and a side view of a face are segmented simultaneously by building separate models for each view, and a combined model for both views. During matching, segmentation is performed using single view models, however shape constraints are applied from a combined model. The approach presented here differs in that the organ shape is modeled simultaneously for all views from the start, contrary to only imposing model constraints from a combined model.

The Multi-View model is constructed by aligning the training shapes for different views separately, and concatenating the aligned shape vectors x_i for each of the N views. A shape vector for N frames is defined as:

$$\mathrm{x} = \left(x_1^{\,T}, x_2^{\,T}, \ldots x_N^{\,T}\right)^T \tag{3.5}$$

By applying a PCA on the sample covariance matrix of the combined shapes, a shape model is computed for all frames simultaneously. The principal model components represent shape variations, which are intrinsically coupled for all views.

For the intensity model, the same applies: an image patch is warped on the average shape for view i and sampled into an intensity vector g_i, the intensity vectors for each single frame are normalized to zero mean and unit variance, and concatenated:

$$\mathrm{g} = \left(g_1^T, g_2^T, \ldots, g_N^T\right)^T \tag{3.6}$$

Analogous to the single frame AAM, a PCA is applied to the sample covariance matrices of the concatenated intensity sample vectors, and subsequently each training sample is expressed as a set of shape- and appearance coefficients. A combined model is computed from the combined shape-intensity sample vectors. In the combined model, the shape and appearance of both views are strongly interrelated, as is illustrated in Figure 3.1.

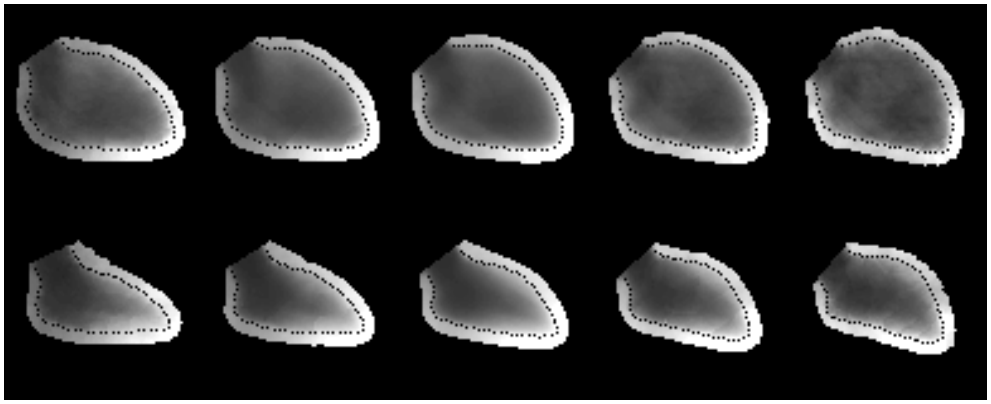

Figure 3.1: First mode of variation for a left ventricle Multi-View AAM, constructed from 70 ED-ES X-ray LV angiograms. Upper row = ED, lower row = ES. The correlation in shape between ED and ES is clearly visible. Also the texture variation, describing mainly the local contrast between the LV and it's embedding around the mitral valve, shows clear similarities for ED and ES.

Estimation of the gradient matrices for computing parameter updates during image matching is performed by applying perturbations on the model, pose, and texture parameters, and measuring their effect on the residual images. Because of the correlations between views in the model, a disturbance in an individual model parameter yields residual images in all views simultaneously. The pose parameters however, are perturbed for each view separately: the model is trained to accommodate for trivial differences in object pose in each view, whereas the shape and intensity gradients are correlated for all views.

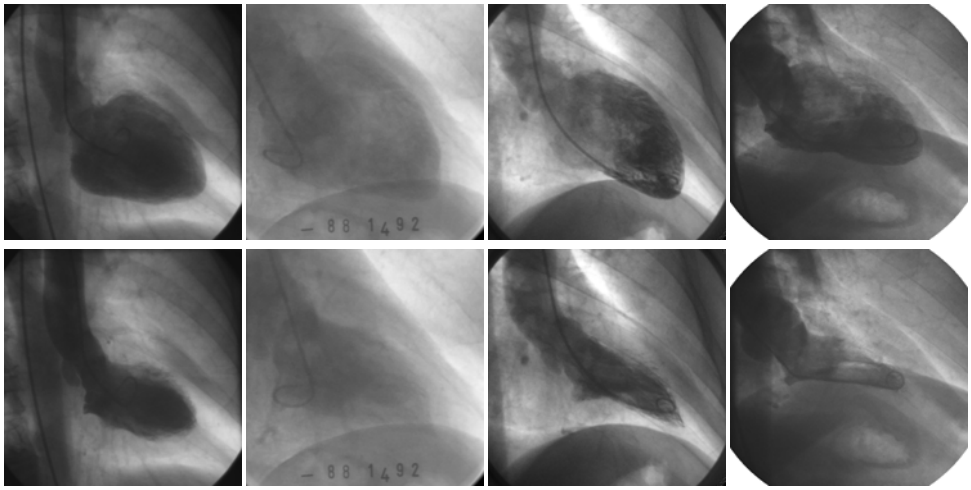

Figure 3.2: X-ray LV angiography example images for ED (upper row) and ES (lower row). From left to right: well defined LV, poor contrast, inhomogeneous distribution of the contrast agent (most apparent in ED) and presence of a diaphragm overlapping the LV.

In the matching procedure, the pose transformation for each view is also applied separately, whereas the model coefficients intrinsically influence multiple frames at a time. Hence, the allowed shape and intensity deformations are coupled for all frames, whereas pose parameter vectors for each view are optimized independently. This is a significant difference as compared to the coupled view AAMs by Cootes *et al.*, where separately trained 2D models are matched to each separate view, and subsequently only the appearance constraints are imposed from a combined appearance model [4].

3.4 Experimental Validation

To determine the clinical utility of the Multi-View AAMs, we investigated two issues:

- To what extent can information from different frames improve overall segmentation performance. To address this, we have tested the Multi-View AAM on X-ray left ventricular angiography images in the ED and ES phase. Though other segmentation methods for LV angiograms have been reported [11,12], these images are notoriously difficult to segment, especially the ES phase. This is mainly due to the fact that in ES a large amount of the contrast agent has already been ejected, therefore border definition of the ventricle is rather poor. For this modality, we expect that the better LV shape definition in ED frames improves the segmentation of ES frames.

- The potential of the Multi-View AAM to segment substantially different geometrical shapes in multiple views. To evaluate this, we selected a combination of cardiac MR short-axis and long-axis views. To our knowledge, this is the first report of an automatic contour detection for endo- and epicardial contours in long-axis cardiac MR views.

3.4.1 X-Ray LV Angiography

The effectiveness of the Multi-View AAM was tested on ED-ES pairs of clinically representative LV angiograms from 70 infarct patients, 140 images in total. Apart from high quality images with good LV definition in both ED and ES, images were selected, in which frequently appearing acquisition artifacts were present (poor LV contrast, inhomogeneous distribution of the contrast agent, presence of a diaphragm overlapping the LV). Figure 3.2 shows representative examples.
An expert manually defined contours in both frames, and point correspondence was defined based on three prominent landmarks: both aortic valve points and the apex. Every contour was equidistantly resampled to 60 points. 14 leave-five-out models were trained on 65 out of 70 ED-ES image pairs, leaving out 5 sets for testing purposes. To speed up the training and matching process and to reduce model dimensionality, all images were subsampled by a factor of 4.

3.4.2 Cardiac MRI

To assess the performance of the Multi-View AAM method for simultaneous segmentation of several different cardiac views with a different geometric definition, the method was evaluated on a commonly acquired combination of cardiac MR views. Usually, during acquisition of a routine cardiac MR patient exam, a two chamber view, a four chamber view and a short-axis stack are acquired following strictly defined acquisition protocols, allowing an optimal depiction of LV anatomy. Following this protocol, image data was acquired from 29 patients with various cardiac pathologies.
The Multi-View AAM was constructed based on the ED two chamber view, the ED four chamber view and the ED mid-ventricular short-axis slice. Endo- and epicardial contours were drawn manually by an expert observer in all views. To maximize the amount of evaluation data, validation and training was performed using a leave-one-out approach. The initial position for the model matching was manually set by indicating the apex and base in the long-axis views, and the LV midpoint in the short-axis views.

3.4.3 Evaluation Method

Matching results for each patient study were first qualitatively scored to three categories: matching success for all views, failure in one view and failure in more than one view. Failures were reported and excluded from quantitative evaluation.

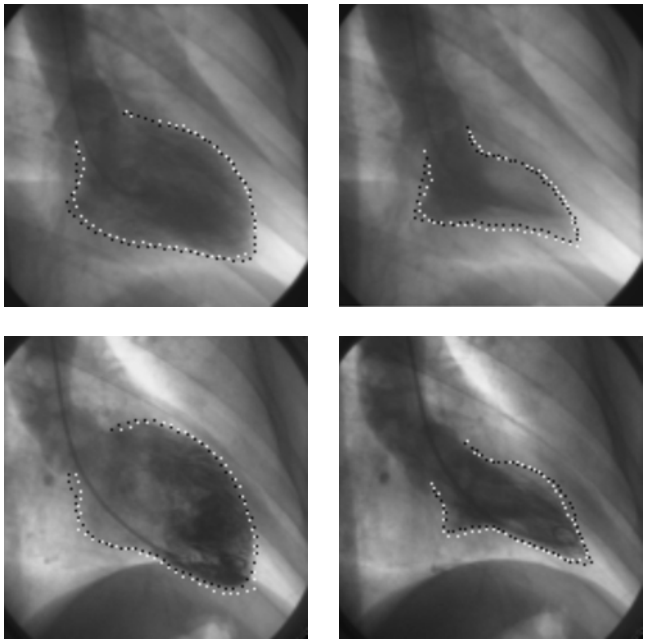

Figure 3.3: Two successful matches for ED (left) and ES (right). Black dotted lines denote the manual contours, white dotted lines represent the model contours. Note that even with inhomogeneous contrast agent distribution (ES image top, ED image below), contours are accurately determined.

On the successful matches, quantitative comparison with expert contours was performed on:

- point-to-curve border positioning errors for the contours as compared to the manually defined expert contours, calculated separately for each view.
- endocardial contour area for each frame separately.
- for the LV angio application, area ejection fraction.

Linear regression was used to determine relationships between manually traced and computer determined values. A two-tailed paired samples t-test was applied to area measurements from automatic and manual contours to investigate systematic errors. A p-value smaller than 0.05 was considered significant.

3.4.4 Results

For the LV angiographic study, the Multi-View AAM yielded borders that agreed closely with the expert defined outlines in both ED and ES in 56 out of 70 patients. In 10 cases, partial failure was observed, where the contour in one frame clearly failed. In 4 cases, neither ED nor ES contours were correctly detected. In total, 122

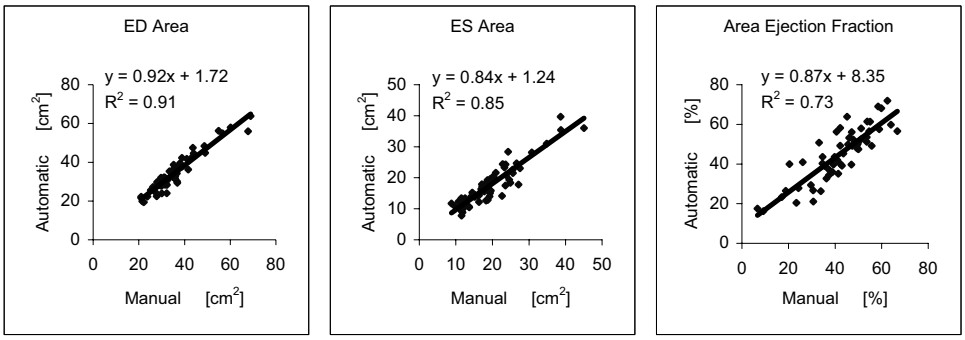

Figure 3.4: Area regression plots for ED (left) and ES (middle) and area ejection fraction (right).

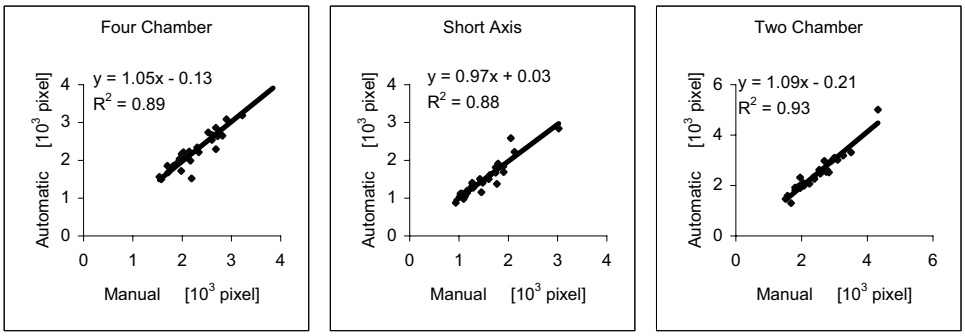

Figure 3.5: Area regression plots for four chamber (left), short-axis (middle) and two chamber (right) cardiac MR views.

	Border positioning errors [pixels]
MRI 2 Chamber	1.7 ± 0.8
MRI 4 Chamber	1.5 ± 0.7
MRI Short axis	1.4 ± 0.7
LV angio ED	6.5 ± 2.8
LV angio ES	8.0 ± 3.7

Table 3.1: Point-to-curve border positioning errors in pixels for the cardiac MR and LV angiography validation studies.

out of 140 images (87%) were successfully segmented, whereas in the other 18 images, manual interaction was required.

In general, for the successful matches, contours showed an excellent agreement with the manually defined contours, even in compelling images with artifacts such as LV-diaphragm overlap, and partial filling. In Figure 3.3, two representative examples of automatically detected contours are given. Border position errors were generally small, and are given in Table 3.1. Area and ejection fraction regressions are given in Figure 3.4. In both ED and ES phases, area errors were slightly, but statistically significantly underestimated ($p<0.001$, relative error for ED 3.5%, for ES 9.4%). The area ejection fraction was slightly overestimated (relative error 7%, $p=0.003$).

The cardiac MR validation yielded 27 successful matches out of 29, and in 2 cases partial failure was observed, where the model drifted away from the LV boundaries in one of the three views. No total failures occurred. Examples of automatically detected contours in the cardiac MR views are given in Figure 3.6. For the contours from successful matches (87 out of 89 images in total, 98%), area correlations between manually and automatically detected contours are given in Figure 3.5, and border positioning errors in Table 3.1. In a paired samples t-test, differences between manually and automatically determined endocardial contour areas were found statistically insignificant for all three views ($p>0.7$ for all views).

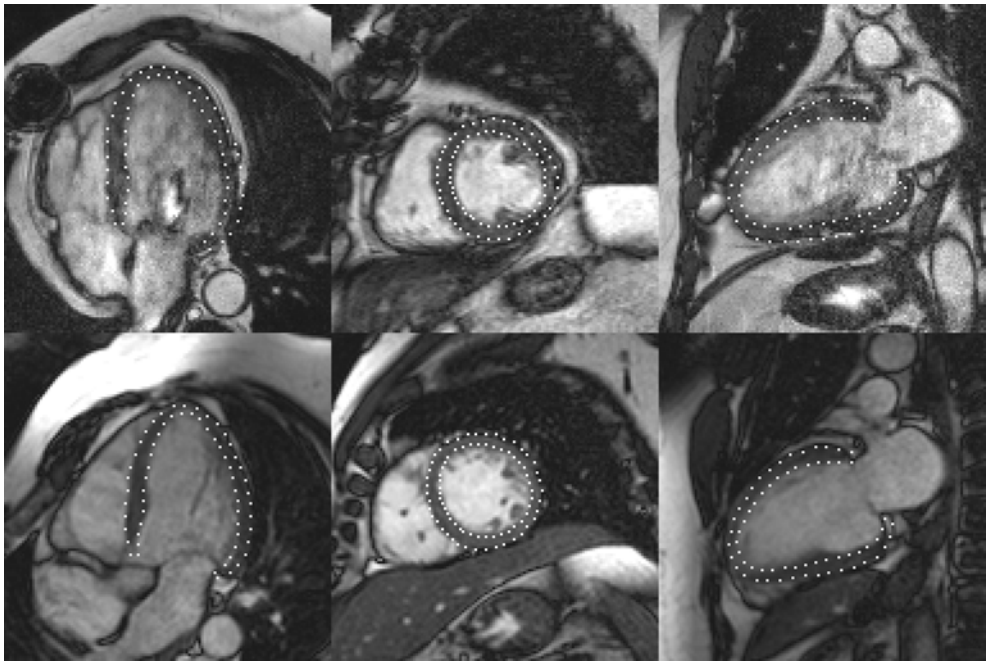

Figure 3.6: Automatically detected contours (white dotted lines) for two patients (top and bottom row) in a four chamber (left), short-axis (middle) and two chamber view.

3.5 Discussion and Conclusions

In general, the presented Multi-View AAM yielded good results in two challenging clinical segmentation problems. Contours were detected with a minimal user interaction to initially position the model, and showed high agreement with manually defined contours. Especially in ES LV angiograms, segmentation results were very good compared to other segmentation methods reported for this modality [11,12]. This good performance in ES images can mainly be attributed to the coupling of information from both ED and ES.

In LV angiography, a success rate of 87% was achieved. Matching failure mainly occurred in cases where contrast was extremely low, when there was a significant overlap between the LV and the diaphragm or in cases of large dilated areas near the apex, as is illustrated in Figure 3.7.

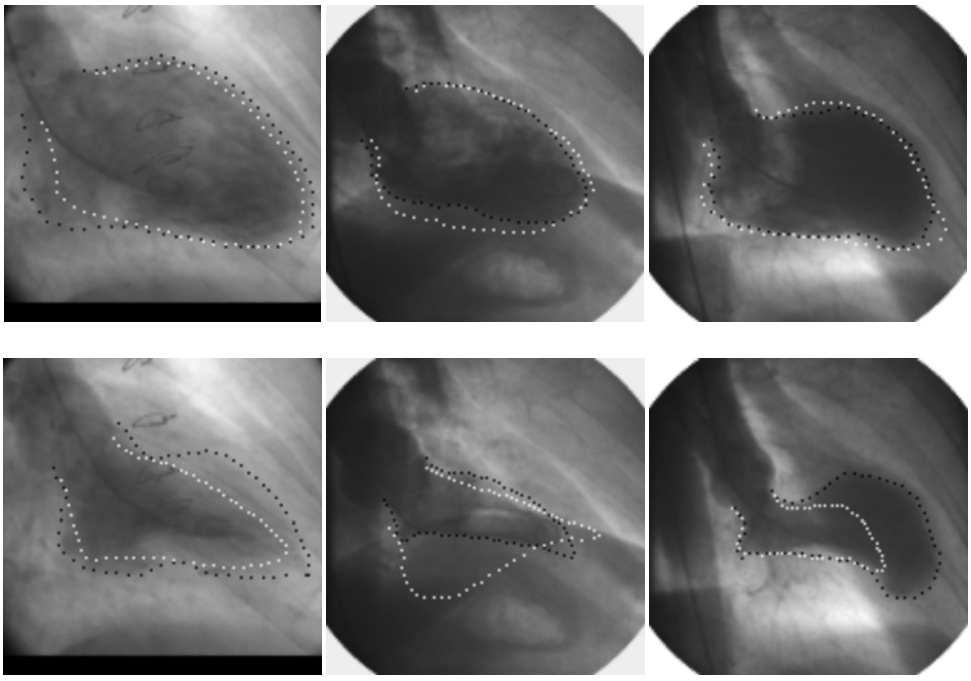

Figure 3.7: Examples of segmentation failures for ED (upper row) and ES (lower row), due to poor contrast (left), overlap between LV and diaphragm (middle) and large dilated areas near the apex (right). The black dotted lines denote the manual contours, the white dotted lines represent the model contours.

Comparison between manually and automatically derived area measurements showed a good correlation, though a slight underestimation of LV area in both ED and ES was present. This underestimation is mainly caused by the lack of dynamic information: a manual observer draws the contours in ED and ES after reviewing

the whole dynamic sequence, whereas automatically generated borders are only based on ED and ES views. When manually examining an entire image run, this motion is used to decide on the border location of the ventricle, especially in "problem areas"; therefore the manual borders are generally drawn slightly wider around the ventricle than visually apparent in only ED and ES. Also, since interpretation and contour drawing in LV angiograms is highly subjective, an assessment of intra- and inter-observer variation inherent to manual contour drawing is ongoing, to compare the accuracy and reproducibility of the automated method for different experts.

The cardiac MR study showed a significantly higher success rate than the LV angiography study: in 98% of the images, a successful match was achieved. This can mainly be attributed to the better definition of the ventricle in cardiac MR views. Though acquisition related artifacts were present in some patient studies (surface coil intensity gradients), overall LV endo- and epicardial contour definition is significantly stronger in the cardiac MR study. Area calculations, which serve as a basis for LV volume estimates, did not differ statistically significantly between manual and automatic analysis. Also for this application, border positioning errors were small (comparable to errors reported in [6]), and well within clinically acceptable margins.

In this study we have tested the Multi-View AAM robustness and performance from a manually set initial position, yielding good results. However, we foresee a further increase in robustness by also coupling the scale of the object in all views, since this is correlated as well between views. This is a topic of current research. Moreover, future research will focus on analysis of Multi-View AAM shape parameters to distinguish between pathologies. We expect the coupling of shape information from different parts of a patient examination to enhance pathology identification. For cardiac MR, methods to automatically position the initial models based on a geometrical thorax template model [13] will be investigated.

In summary, we conclude that the Multi-View AAM presented here combines a high robustness with clinically acceptable accuracy. It demonstrated good automatic segmentation results for two substantially different and novel clinical applications. A cardiac MR case study showed the utility to simultaneously segment different geometrical shapes, and a case study on X-ray LV angiography proving that poor ventricle definition in one view (ES) can be resolved by information from a corresponding (ED) view.

References

[1] T. F. Cootes, G. J. Edwards, and C. J. Taylor, "Active appearance models," *Proceedings of the European Conference on Computer Vision*, H. Burkhardt and B. Neumann, Eds., vol. 2, Berlin: Springer Verlag, 1998, pp. 484-498.

[2] T. F. Cootes, C. Beeston, G. J. Edwards, and C. J. Taylor, "A Unified Framework for Atlas Matching Using Active Appearance Models," *Proceedings of Information Processing in Medical Imaging*, Kuba, Samal and Todd-Pokropek, Eds, vol. 1613, pp. 322-333, 1999.

[3] T. F. Cootes and C. J. Taylor, "Statistical models of appearance for computer vision," Online available: *http://personalpages.manchester.ac.uk/staff/timothy.f.cootes/Models/app_models.pdf*

[4] T.F. Cootes, G.V. Wheeler, K.N. Walker, C.J. Taylor, "View-based active appearance models," *Image and Vision Computing*, vol. 20, no. 9-10, pp. 657-664, 2002.

[5] T.F.Cootes, P.Kittipanya-ngam, "Comparing Variations on the Active Appearance Model Algorithm," *Proceedings of British Machine Vision Confererence*, vol.2, pp. 837-846, 2002.

[6] S. C. Mitchell, B. P. F. Lelieveldt, R. J. Van der Geest, H. G. Bosch, J. H. C. Reiber, and M. Sonka, "Multistage hybrid active appearance model matching: segmentation of left and right ventricles in cardiac MR images," *IEEE Transactions on Medical Imaging*, vol. 20, no. 5, pp. 415-423, 2001.

[7] H.H. Thodberg, "Hands on Experience with Active Appearance Models," *Proceedings of SPIE Medical Imaging*, vol. 4684, pp. 495-506, 2002.

[8] J. G. Bosch, S. C. Mitchell, B. P. F. Lelieveldt, F. Nijland, O. Kamp, M. Sonka, and J. H. C. Reiber, "Automatic segmentation of echocardiographic sequences by active appearance motion models," *IEEE Transactions on Medical Imaging*, vol. 21, no. 11, pp. 1374-1383, 2002.

[9] R. Beichel, G. Gotschuli, E. Sorantin, F. Leberl, M. Sonka, "Diaphragm Dome Surface Segmentation in CT Data Sets: A 3D Active Appearance Model Approach," *Proceedings of SPIE Medical Imaging*, vol. 4684, pp. 475-484, 2002.

[10] S.C. Mitchell, J.G. Bosch, B.P.F. Lelieveldt, R.J. van der Geest, J.H.C. Reiber, M. Sonka, "3D Active Appearance Models: Segmentation of Cardiac MR and Ultrasound images," *IEEE Transactions on Medical Imaging,* vol. 21, no. 9*,* pp. 1167-1178*,* 2002.

[11] S. Tehrani, T. E. Weymouth, and G. B. J. Mancini, "Model generation and partial matching of left ventricular boundaries," *Proceedings of SPIE Medical Imaging*, vol. 1445, pp. 434-445, 1991.

[12] P. Lilly, J. Jenkins, and P. Bourdillon, "Automatic contour definition on left ventriculograms by image evidence and a multiple template-based model," *IEEE Transactions on Medical Imaging*, vol. 8, no. 2, pp. 173-185, 1989.

[13] B. P. F. Lelieveldt, M. Sonka, L. Bolinger, T. D. Scholz, H. W. M. Kayser, R. J. van der Geest, and J. H. C. Reiber, "Anatomical Modeling with Fuzzy Implicit Surface Templates: Application to Automated Localization of the Heart and Lungs in Thoracic MR Volumes." *Computer Vision and Image Understanding*, vol. 80, pp. 1-20, 2000.